

# Protein folding is governed by memory-dependent friction

Benjamin A. Dalton, Cihan Ayaz, Lucas Tepper, and Roland R. Netz  
*Fachbereich Physik, Freie Universität Berlin, 14195 Berlin, Germany*

When described by a low-dimensional reaction coordinate, the rates of protein folding are determined by free energy barriers, which separate folded and unfolded states, and by friction, which results from interactions with the solvent environment and internal, intra-molecular interactions. While it is relatively straightforward to measure free energy barriers, a direct evaluation of friction is far more elusive. Here, using memory-kernel extraction methods, we directly calculate the friction acting on a protein, which accounts for both external and internal contributions. By employing a generalised Langevin equation (GLE) formalism to describe the dynamics of the fraction of native contacts reaction coordinate  $Q$ , we evaluate friction kernels for eight fast-folding proteins, taken from a published set of large-scale, molecular dynamics protein simulations. Our results reveal that friction is more important than the free energy barriers in determining protein folding rates, particularly for larger proteins. We show that proteins typically fold in an accelerated kinetics regime, which is a purely non-Markovian effect.

## INTRODUCTION

In many cases, protein functionality depends on proteins folding successfully into a specific three-dimensional conformational state. Protein folding requires that a linear polypeptide chain is driven to explore conformation space by interactions with a solvating environment, and is shaped by both solvent interactions and internal interactions between amino acids. Folding and unfolding typically occur over a free energy landscape [1–6], with distinct states separated by free energy barriers, often of the order of a few  $k_B T$ 's in height. Theories for describing protein folding are often phrased as reaction rate theories with an explicit dependence on the free energy barrier of separation, and friction. An accurate understanding of the kinetics of barrier-crossing reactions is not only important for describing protein folding but is essential in many other fields, such as nucleation theory and chemical kinetics. Reaction rate theory dates back to Arrhenius, who, in 1889, [7] showed that the transition times between reactant and product scale according to  $\kappa e^{U_0/k_B T}$ , where  $U_0$  is the height of the energy barrier separating the two states. The pre-factor  $\kappa$ , however, depends on both the free energy profile and friction. Building on the transition state theory of Eyring, [8], Kramers was the first to include an explicit dependence on solvent friction [9]. The friction in Kramers theory is frequency-independent, suggesting that the environment of the reacting system relaxes infinitely fast compared to the relevant time scales of the reacting system. Regardless of its simplicity, Kramers theory predicts reaction rates in both the over-damped and inertia-dominated regimes well and is sufficient for describing many systems. Various advancements have been made that bridge the over-damped and inertia-dominated regimes, with many accommodating the finite environmental relaxation times [10–14]. In the case of proteins, it is known that friction is determined by a combination of interactions with the solvent environment and internal intramolecular interactions [15–17], and that finite relaxation occurs [18]. A

direct evaluation of the friction acting on a protein has not been possible and approaches have rather relied on determining friction from memoryless reaction rate theory [19–21]. In this paper, we directly extract the friction acting on the conformational dynamics of proteins from molecular dynamics simulation trajectories, which accounts for both internal and external friction contributions, and finite relaxation times.

We evaluate friction for eight fast-folding proteins, obtained from previously published large-scale molecular dynamics simulation trajectories [22]. These cutting-edge simulations, performed by the Shaw group using the purpose-built Anton super-computer [23, 24], represent a breakthrough in the simulation-of-scale, enabling all-atom simulation of proteins that would not otherwise be practically possible. The lengths of the proteins range between 10 and 80 amino-acid residues, and the simulation times between approximately 100  $\mu$ s and 3 ms. The result is a diverse protein data set, comprised of mixtures of  $\alpha$ -helix and  $\beta$ -hairpin secondary structures, and an assortment of tertiary structures, where all proteins execute a multitude of folding and unfolding events.

We analyse all protein trajectories in the framework of a non-Markovian, generalised Langevin equation (GLE). The GLE is a low-dimensional representation of some higher dimension system. In the present case, we collapse the all-atom dynamics of the composite water-protein systems onto a one-dimensional reaction coordinate. This process of dimension reduction is known as projection [25, 26]. We project the all-atom trajectories, as provided by the Shaw group, onto a well-known fraction of native contacts reaction coordinate [27] with soft cut-off  $Q$  [28], and hence extract friction memory kernels from  $Q(t)$ . Free-energy profiles and friction are a property of dimension reduction, and are therefore unique to a given reaction coordinate. The extracted friction kernels encode dissipation across a spread of time scales, representing the finite relaxation rates of solvent processes and internal reconfigurations, as far as they are represented in  $Q(t)$ . Consequently, the friction kernel contains the information for the full friction acting on the reaction coordi-

nate. From the free energy landscape and friction kernels, we derive predictions for the folding times on different levels of reaction rate theory and compare to the folding times measured in the simulation. In doing so, we show that the best prediction for the measured folding times is given by a multi-time-scale, non-Markovian theory, which has hitherto only been applied to the characterisation of model systems [13, 14]. This validation is only possible owing to the long simulation times and diverse range of proteins that comprise the extensive protein data set. We show that the memory decay-times, i.e., the duration of memory effects, are significantly long for all proteins in this set, in some instances as long as the folding times. This indicates that even for  $Q$ , which is typically considered by other measures to be a good reaction coordinate [28], must be considered as a poor reaction coordinate, when judged according to its non-Markovianity. Finally, we also show that, for this particular set of proteins, friction is more important than free-energy barriers in determining folding times, and that this dominance of friction increases for larger proteins. Taken together, our findings suggest that, when represented by a low-dimensional reaction coordinate, the conformational dynamics of proteins are dominated by friction and should be treated as non-Markovian in nature.

## RESULTS

**Extracting friction from protein simulations:** The PDB structures for the eight proteins, along with the number of residues that make up each chain, are shown in Fig. 1A. The fraction of native contacts reaction coordinate  $Q$  is described in detail in the Materials and Methods section. In brief,  $Q$  provides a measure for the deviation of a given state away from some native reference state, which typically represents the folded state.  $Q$ , which is evaluated in connectivity space and is therefore unitless, is closer to  $Q = 1$  in the folded state and closer to  $Q = 0$  when unfolded. For the set of eight proteins, we identify a native state and hence project each corresponding all-atom trajectory onto a unique  $Q(t)$ . In Fig. 1B, we show a 250  $\mu$ s trajectory segment for the  $\alpha_3$ D protein. The distinct folded and unfolded states are discernible, located at  $Q_f = 0.75$  and  $Q_u = 0.51$  respectively, separated by a barrier at  $Q_b = 0.66$ . In the magnification windows set above the trajectory, we indicate schematic examples for the calculation of first-passage times  $\tau_{FP}$  and transition path times  $\tau_{TP}$ . Throughout this paper, we consider folding transitions as leading from the unfolded state minimum to the barrier top ( $Q_u \rightarrow Q_b$ ), and unfolding transitions as leading from the folded state minimum to the barrier top ( $Q_f \rightarrow Q_b$ ). This accounts for the strong asymmetries observed in the free energy profiles for the eight proteins. In the left magnification, we identify a sequence of folding first-passage events. The mean of all such first-passage events, taken over the full trajectory, are accumulated to evaluate the mean first-

passage time  $\tau_{MFP}^{MD}$  for the folding reaction. Likewise, we evaluate the unfolding times as the mean of all first-passage events from  $Q_f$  to  $Q_b$ . In the right magnification, we show an example folding transition path, connecting the unfolded state minimum to the barrier top. A mean transition path time  $\tau_{MTP}$  is simply the mean for all such transition path durations for either folding or unfolding transition. From the trajectories of  $Q(t)$  for each protein, we calculate the free energy profile  $U(Q)$  acting on the reaction coordinate. In Fig. 1C, we show  $U(Q) = -k_B T \log[\rho(Q)]$  for the  $\alpha_3$ D protein, where  $\rho(Q)$  is the probability density for  $Q(t)$ ,  $k_B$  is Boltzmann's constant, and  $T$  is the system temperature, which has a unique value for each protein. We show the free energy profiles for all proteins in the SI (Section 6). All free energy profiles are asymmetric, such that the barrier heights faced by the folded and unfolded states ( $U_{0,u}$  and  $U_{0,f}$ ) are not equal. Likewise, the distances in reaction-coordinate space from the minima to the barrier top ( $L_f$  and  $L_u$ ) are also different.

Central to this paper is the extraction of time-dependent friction kernels  $\Gamma(t)$  from the  $Q(t)$  trajectories for each of the eight proteins. We describe the stochastic dynamics of  $Q(t)$  by the one-dimensional generalised Langevin equation (GLE):

$$m\ddot{Q}(t) = - \int_0^t \Gamma(t-t')\dot{Q}(t')dt' - \nabla U[Q(t)] + F_R(t), \quad (1)$$

where  $\Gamma(t)$  is the friction memory kernel,  $F_R(t)$  is the random force term satisfying the fluctuation-dissipation theorem  $\langle F_R(t)F_R(t') \rangle = k_B T \Gamma(t-t')$ ,  $m$  is the effective mass of the reaction coordinate, and  $U(Q)$  is the free energy profile. Eq. 1 neglects non-linear friction and is therefore approximate [29]. There are various methods for extracting dynamic friction from discrete time-series trajectories [30–32]. We describe the method used here for extracting  $\Gamma(t)$  from  $Q(t)$  in detail in the SI (Section 2). In short, we directly extract the running integral of the memory kernel  $G(t) = \int_0^t \Gamma(t')dt'$  using a Volterra extraction scheme, which is suitable for arbitrary, non-linear, free-energy profiles  $U(Q)$  [33, 34]. The memory kernel is then given by  $\Gamma(t) = dG(t)/dt$ , which is evaluated numerically. The memory kernel for the  $\alpha_3$ D protein, normalised by  $\Gamma(0)$ , is shown in Fig. 1D. The dynamics of the  $\alpha_3$ D protein exhibit significant memory effects, which is clear from the inset, which shows that the running integral  $G(t)$  plateaus after about 10  $\mu$ s. We show the memory kernels for all proteins in the SI (Section 7).

**Scaling of GLE parameters with system size:** Having extracted the full time-dependent friction kernel via  $G(t)$ , we also have access to the zero-frequency friction  $\gamma = G(t \rightarrow \infty)$ , which we refer to throughout as the total

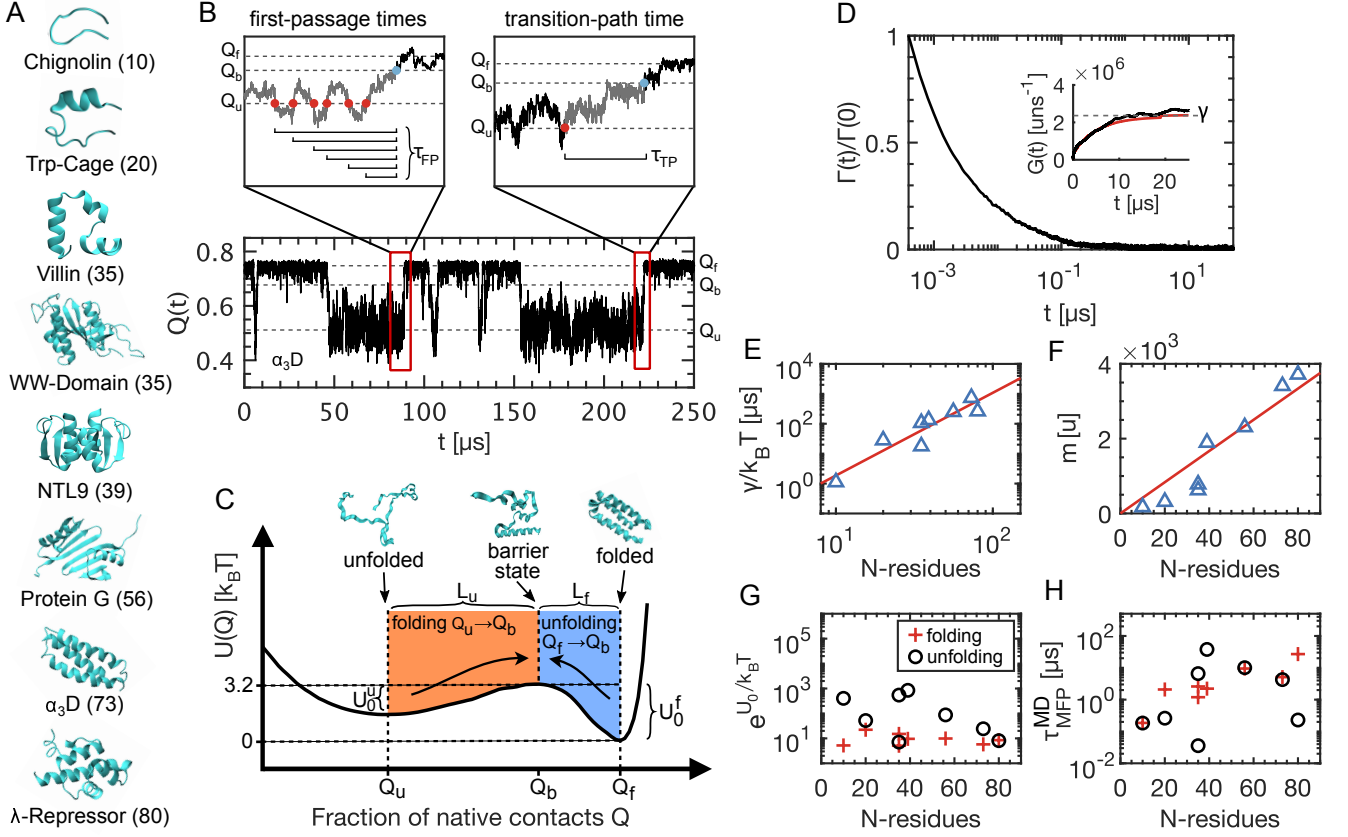


FIG. 1. The folding and unfolding of eight fast-folding proteins. A) PDB entries for eight proteins, with the number of amino acids in each protein. B) 250  $\mu\text{s}$  trajectory segment for the  $Q(t)$  reaction coordinate ( $\alpha_3\text{D}$  protein). Left magnification: a sequence of folding first-passage times, from the unfolded state  $Q_u$  to the barrier top  $Q_b$ . Right magnification: an example folding transition path and corresponding transition path time. C) Free energy profile for the  $\alpha_3\text{D}$  protein. Configuration snapshots show example folded and unfolded states, with an example barrier state.  $Q_u$  and  $Q_b$  are the reaction coordinate values in the folded and unfolded states, respectively.  $Q_b$  is the transition barrier top. Asymmetric barrier heights are also indicated. For  $\alpha_3\text{D}$ , the barrier faced by the unfolded protein,  $U_0^u = U(Q_b) - U(Q_u) = 3.2 k_B T$ , is less than the barrier faced by the folded protein  $U_0^f = U(Q_b) - U(Q_f) = 1.8 k_B T$ . The distance from the unfolded state to the barrier top  $L_u = Q_b - Q_u$  is greater than the distance from the folded state to the barrier top  $L_f = Q_f - Q_b$ . D) Normalised GLE memory kernel, extracted from  $Q(t)$  for the  $\alpha_3\text{D}$  protein. Running integral  $G(t)$  and the limiting total friction  $\gamma$  (inset - dashed line). Running integral of an exponential series fit to  $\Gamma(t)$  (red curve). E) Total friction  $\gamma$  for each protein, plotted as a function of the number of residues  $N$ , divided by  $k_B T$  to account for unique temperature  $T$  (power law with exponent  $\sim 2.8$  (red line)). F) Effective mass  $m$ , plotted as a function of  $N$  (linear fit with a gradient of 41 u per residue (red line)). G) and H) show the Arrhenius factor  $e^{U_0/k_B T}$  and barrier crossing times  $\tau_{\text{MFP}}^{\text{MD}}$  as a function of protein lengths folding and unfolding transitions individually.

friction. In Fig. 1E, we show  $\gamma$  for each protein, plotted as a function of the number of residues in each chain  $N$ . To account for each system having a unique temperature, we divide by  $k_B T$ . We fit a power law and find that  $\gamma/k_B T = 3.2 \times 10^{-3} N^{2.8} \mu\text{s}$  (red line) [35]. If the friction on  $Q$  is determined solely by solvent interactions, we would expect approximately linear scaling. This is the case for the effective mass, which we calculate using the equipartition theorem  $m = 2k_B T / \langle \dot{Q} \rangle^2$  (Fig. 1F). The linear scaling of  $m$  (red line) indicates that the effective mass of  $Q$  is largely determined by the molecular mass of the protein chain [29]. The power-law scaling of  $\gamma$  suggests that intramolecular interactions are more influential for longer chains, owing to the reptation-like reconfiguration dynamics [36]. Interestingly, increasing

chain length does not appear to directly couple to free energy barrier heights. The Arrhenius barrier terms  $e^{U_0/k_B T}$ , plotted in Fig. 1G, show that the hindrance to protein folding imposed by free energy barriers is remarkably uncorrelated with the size of a protein. The folding and folding kinetics, however, which we quantify as the mean first-passage times  $\tau_{\text{MFP}}^{\text{MD}}$  (Fig. 1H), do increase with  $N$ . Therefore, whereas the separation barrier heights do not appear to increase with  $N$ , the barrier crossing times do. Overall, Fig. 1E-H tells us that, when projected onto  $Q$ , friction plays a dominant role in governing the dynamics and kinetics of protein folding and that the free energy profiles, while certainly also essential, appear to be less influential than friction in determining protein folding reaction rates, as will be

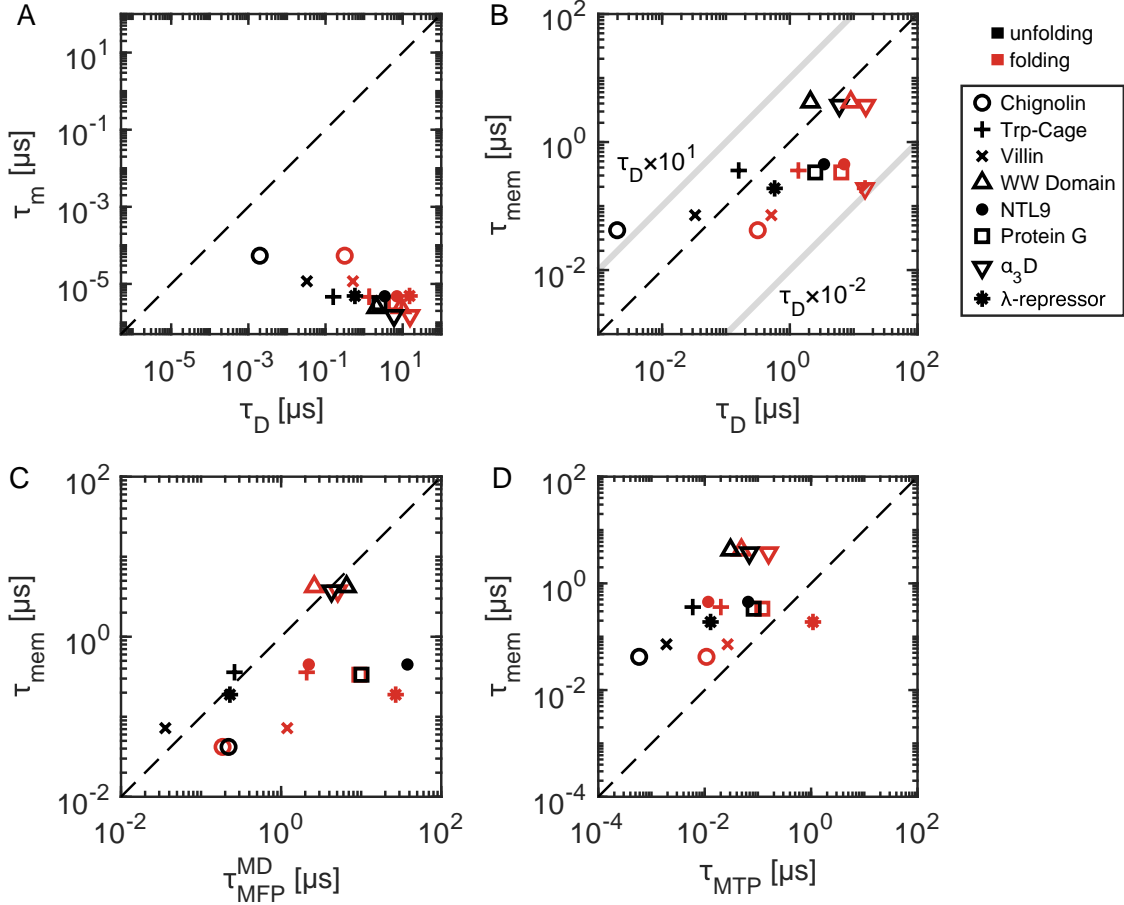


FIG. 2. Comparison of relevant time scales for protein folding and unfolding dynamics and kinetics. A) The inertia time scales  $\tau_m$  compared to the diffusion times  $\tau_D$ , showing that all systems are in the over-damped regime. B) Memory decay time-scale  $\tau_{\text{mem}}$ , calculated from the first moment of the memory kernel  $\Gamma(t)$ , compared to the diffusion times  $\tau_D$ . The light grey lines indicate the bounding regime for  $\tau_{\text{mem}}$  between  $\tau_D \times 10^{-2}$  and  $\tau_D \times 10^1$ , which is the domain in which memory-induced kinetic speed-up is expected. C) Memory times  $\tau_{\text{mem}}$  compared to the folding and unfolding times, expressed as the mean first passage times  $\tau_{\text{MFP}}^{\text{MD}}$ . D) Memory times compared to the transition path times  $\tau_{\text{MTP}}$  leading from the folded and unfolded state minima to the barrier tops. The broken lines in each plot indicate exact equivalence, or correlation, between the respective quantities.

correlated more quantitatively further below.

### Memory duration is significant in protein folding:

As well as proving the total friction for  $Q$ , the extraction of  $\Gamma(t)$  provides a time scale for the sustain of memory effects. Furthermore,  $\gamma$  can be used predictively, to evaluate other key dynamic time scales. How do these time scales compare? The inertia time  $\tau_m = m/\gamma$  is the time scale beyond which the system becomes diffusive. The diffusion time:

$$\tau_D = \frac{\gamma L^2}{k_B T}, \quad (2)$$

is the time taken for a Brownian particle to diffuse over a characteristic distance  $L$  in the absence of free energy gradients. Both  $\tau_m$  and  $\tau_D$  depend on  $\gamma$ . A system is in an over-damped regime when  $\tau_m \ll \tau_D$ . This condition is met for all eight proteins, as can be seen in Fig. 2A, for both  $L_u$  and  $L_f$ . One ambiguous case is Chignolin

unfolding, for which  $\tau_m/\tau_D = 0.027$ . For Chignolin, both the characteristic length in the folded state  $L_f$ , and  $\gamma$ , are considerably small.

By comparing  $\tau_D$  to the decay times of the extracted memory kernels, we can intuit whether we expect memory effects to influence barrier crossing processes. Memory-dependent friction typically exhibits cascading time scales, meaning that  $\Gamma(t)$  is multi-modal, with time scales spanning many orders of magnitude [33]. To assign a single effective time-scale to the memory decay  $\tau_{\text{mem}}$ , we evaluate the first-moment for the set of extracted memory kernels:  $\tau_{\text{mem}} = \int_0^\infty t\Gamma(t)dt / \int_0^\infty \Gamma(t)dt$ . In the SI (Section 3), we address the issue of discretization due to the intrinsically low time resolution of the MD data with a highly resolved trajectory for an  $\alpha$ -helix forming Ala<sub>9</sub> homo-peptide chain. Fig. 2B shows that overall, memory times are non-negligible when compared to diffusion times. Memory times accelerate barrier crossing kinetics in the range  $1 \times 10^{-2} < \tau_{\text{mem}}/\tau_D < 1 \times 10^1$

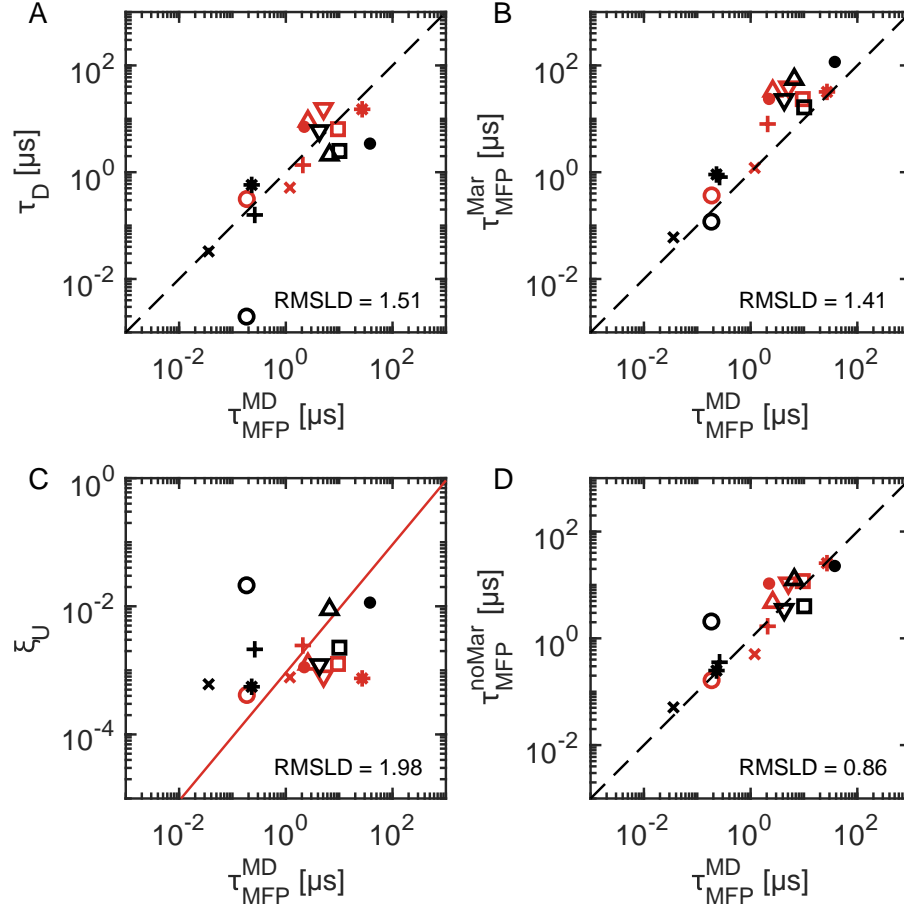


FIG. 3. Predicting folding and unfolding times. A) Diffusion times  $\tau_D$ , according to Eq. 2, compared to the measured barrier crossing times  $\tau_{\text{MFP}}^{\text{MD}}$ . B) Markovian predictions  $\tau_{\text{MFP}}^{\text{Mar}}$ , according to Eq. 3, for barrier crossing times on exact free-energy profiles. C) Free energy factor  $\xi_U$ , accounting for the effects of the free-energy landscape on the reaction time, according to Eq. 3. D) Non-Markovian predictions  $\tau_{\text{MFP}}^{\text{noMar}}$ , according to Eq. 5, for the barrier crossing times, evaluated by correcting  $\tau_{\text{MFP}}^{\text{Mar}}$  to account for non-Markovian effects, using the correction factor  $\xi_{\text{noMar}}$ , as given by Eq. 4. Root-mean-squared logarithmic deviations score the population deviation from exact agreement with the measured  $\tau_{\text{MFP}}^{\text{MD}}$  for A), B), and D) (dashed lines), and the optimal linear regression in C) (red line). See Fig. 2 for symbol legend.

[12–14], which is indicated on Fig. 2B, where the Grote-Hynes theory is valid [11]. In Fig. 2C, we see that memory times are at most comparable to the reaction times, but are typically shorter, indicating that  $Q$  is a poor reaction coordinate. The overall concurrence between  $\tau_{\text{mem}}$ ,  $\tau_D$ , and  $\tau_{\text{MFP}}^{\text{MD}}$  reveals a coupling between memory effects and folding kinetics.

The comparison between memory times and transition path times is particularly revealing. Transition paths are the segments of a trajectory where the protein actually executes the reconfiguration from one specific state to another target state. Transition paths are of much interest since they provide information about the actual folding mechanisms of a protein, and have been studied extensively in experiments [37–40], and in the context of simulation and theory [22, 28, 41–45]. In Fig. 2D, we show that for all proteins, memory times are long compared to transition path times. This is significant for two reasons. Firstly, it tells us that entire transitions

either fold or unfold under the influence of memory effects that linger from the preceding state. Secondly, it explains why the approximate, position-independent form of Eq. 1 works. Even describing the dynamics of  $Q$  as having distinct memory dependence on separate sides of the barrier would be neutralised since memory effects can last for as much as two orders of magnitude longer than the time required to move between states. Therefore, we must keep in mind the overwhelming dominance of the duration of memory effects compared to the time required to traverse a free energy barrier.

**Non-Markovian models predict protein folding times:** From the simulation trajectories, we measure the folding and unfolding times, evaluated via the mean first-passage times  $\tau_{\text{MFP}}^{\text{MD}}$ . Since we can also extract the total friction directly from the simulation trajectories, we can parametrise various theoretical estimates for folding and unfolding times, and hence compare to the mea-



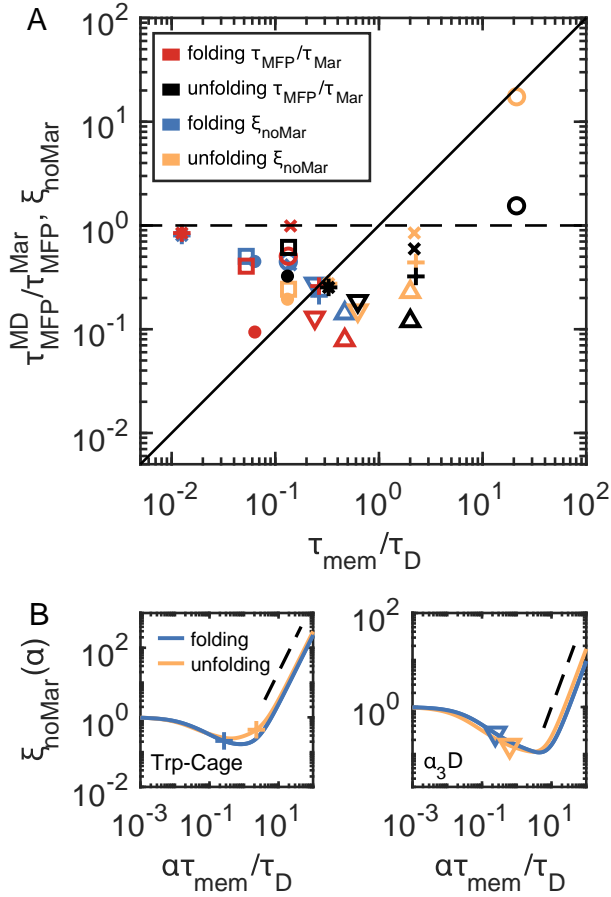


FIG. 4. Barrier crossing times indicate memory-induced speed-up. A) Deviations from Markovian barrier crossing kinetics, plotted as a function of scaled memory times  $\tau_{\text{mem}}/\tau_D$ , for the folding and unfolding of all eight proteins. Rescaled MD simulation values for each protein ( $\tau_{\text{MFP}}^{\text{MD}}/\tau_{\text{MFP}}^{\text{Mar}}$ , red and black symbols) are compared to multi-modal, non-Markovian prediction ( $\xi_{\text{noMar}}$ , blue and yellow symbols). See Fig. 2 for symbol legend. B) Multi-modal, non-Markovian predictions  $\xi_{\text{noMar}}$  plotted as a function of rescaled first-moment memory time  $\alpha\tau_{\text{mem}}$  for two examples: Trp-Cage and  $\alpha_3\text{D}$ . The symbols are for  $\alpha = 1$ , which coincide with the appropriate  $\xi_{\text{noMar}}$  values in A). Dashed lines indicate quadratic scaling  $\sim (\tau_{\text{mem}}/\tau_D)^2$  for the long memory-time slow-down regime.

sured simulation values. To quantify the population-wide deviation away from the measured  $\tau_{\text{MFP}}^{\text{MD}}$ , we use the root-mean-square logarithmic deviation (RMSLD). We collect the folding and unfolding times into a single set and we logarithmically weight each value to balance contributions from the spread of time scales (see SI - Section 10). The population-wide deviations are given by  $\text{RMSLD} = \sqrt{\sum_{i=1}^N (\log(\tau_{\text{MFP},i}^{\text{MD}}) - \log(\tau_{\text{MFP},i}^{\text{theo}}))^2 / N}$ , where  $\tau_{\text{MFP},i}^{\text{MD}}$  is the measured value from MD,  $\tau_{\text{MFP},i}^{\text{theo}}$  is the theoretical predicted value for a given method, and  $N = 16$  is the total number of reactions. For the diffusion times  $\tau_D$ , we determine a total logarithmic deviation of 1.51. This result is remarkable since it completely ne-

glects the free energy barriers, depending only on the friction and characteristic lengths. This result implies that friction alone provides a good approximation for protein folding times. A Markovian prediction, which explicitly accounts for the extracted free energy profiles, is given by:

$$\begin{aligned} \tau_{\text{MFP}}^{\text{Mar}}(Q_a|Q_b) &= \tau_D \int_{Q_a}^{Q_b} e^{\beta U(x)} \left[ \int_{-\infty}^x e^{-\beta U(y)} \frac{dy}{L} \right] \frac{dx}{L} \\ &= \tau_D \xi_U, \end{aligned} \quad (3)$$

where  $\beta = 1/k_B T$ . Eq. 3 assumes constant friction across  $Q$  and evaluates the mean first-passage times between any two points on the free energy landscape,  $Q_a$  and  $Q_b$ . In the case of folding reactions, we calculate  $\tau_{\text{MFP}}^{\text{Mar}}(Q_u|Q_b)$ . For unfolding, we reflect the free energy profile  $U(Q) \rightarrow U(Q_{\text{max}} - Q)$  and hence calculate  $\tau_{\text{MFP}}^{\text{Mar}}(Q_f|Q_b)$ . Again, we see that the population-wide prediction is good (Fig 3B), but with a general trend that the Markovian predictions are slow compared to the MD data. From Eq. 3,  $\xi_U$  is a factor that depends on the exact free energy profile. The RMSLD value of 1.41 for the Markovian predictions shows that the contribution due to  $\xi_U$  is small. We emphasised this in Fig 3C, where we show the population of  $\xi_U$  values corresponding to the set of barrier crossing times. Here, we calculate an RMSLD value of 1.98 using linear regression (red line). This large spread of  $\xi_U$  values confirms that by explicitly including free energy profiles, we can not improve upon a prediction for the barrier crossing times that is given solely by friction.

Can we improve these predictions by taking the proposed non-Markovianity into account? Using a simplified non-Markovian model with multi-modal memory in symmetric free energy profiles with parabolic barriers [13, 14], we determine a non-Markovian correction factor  $\xi_{\text{noMar}}$ , which is given by:

$$\xi_{\text{noMar}} = \frac{\tau_{\text{MFP}}^{\text{H}}(\tau_D, U_0, \{\gamma_i\}, \{\tau_i\}, \tau_{\text{m}})}{\tau_{\text{MFP}}^{\text{H}}(\tau_D, U_0, \{\gamma_i\}, 0, 0)}. \quad (4)$$

$\tau_{\text{MFP}}^{\text{H}}$  is the barrier-crossing time predicted by a heuristic cross-over formula. This term contains a series of  $M$  over-damped contributions, which dominate when memory times are short compared to the diffusion times, and  $M$  energy-diffusion contributions, which dominate when memory times are large. The exact nature of these contributions is described in detail in the materials and methods section (see Eqs. M2 - M4). Briefly, we fit the extracted memory kernels with an exponential series  $\Gamma(t) \approx \sum_{i=1}^M (\gamma_i/\tau_i) \exp(-t/\tau_i)$  (see SI - Section 7), resulting in a set of  $M$  amplitudes  $\{\gamma_i\}$  and time-scales  $\{\tau_i\}$ . For Chignolin,  $M=2$ . For all other proteins,  $M=3$ . The denominator in Eq. 4 represents the memoryless, Markovian limit, where the mass is assumed to be zero and the

memory time scales are infinitely short. The results for the corrected Markovian predictions:

$$\tau_{\text{MFP}}^{\text{noMar}} = \xi_{\text{noMar}} \tau_{\text{MFP}}^{\text{Mar}}, \quad (5)$$

are given in Fig 3D. We see an overall improvement, except for the case of Chignolin unfolding, Villin folding, and Protein G unfolding. Population-wide, we see a significant improvement in the RMSLD, yielding a value of 0.86. While the errors are still quite large, we recall that aside from the sets  $\{\gamma_i\}$  and  $\{\tau_i\}$ , which are taken from the extracted memory kernels,  $\xi_{\text{noMar}}$  is a fit-free quantity, with all parameters extracted from the MD trajectories. Non-Markovian reaction rate theory represents a significant improvement when predicting protein folding times.

**Proteins fold in the memory-induced speed-up regime:** In reactive systems, memory effects can result in either the speed-up or slow-down of reaction times, when compared to a memoryless analog, depending on the memory time scales [12–14]. For our analysis,  $\tau_{\text{MFP}}^{\text{Mar}}$  represents a memoryless analogue to the actual, measured system  $\tau_{\text{MFP}}^{\text{MD}}$ . The ratio of  $\tau_{\text{MFP}}^{\text{MD}}/\tau_{\text{MFP}}^{\text{Mar}}$  reveals deviations from pure Markovian behaviour. If we rescale memory times by the corresponding diffusion times, we have a relative measure for the duration of memory decay compared to the underlying transport time over the reactive distance. By plotting  $\tau_{\text{MFP}}^{\text{MD}}/\tau_{\text{MFP}}^{\text{Mar}}$  against the rescaled memory times  $\tau_{\text{mem}}/\tau_{\text{D}}$  for all proteins, we observe the deviation from pure Markovianity over the range of extracted memory times. The red (folding) and black (unfolding) symbols in Fig. 4A reveal a speed-up regime across the population of proteins. In the short and long memory-time limits, reaction times trend to Markovian behaviour, which is expected from previous works [13, 14]. Memory-induced speed-up has already been observed in short homo-peptide chains [33]. Our results indicate that memory effects are present in larger proteins and that these effects likely explain the observed acceleration of the folding and unfolding reactions.

Using  $\xi_{\text{noMar}}$  predictively, we can demonstrate that the reaction-acceleration effects are induced by memory effects.  $\xi_{\text{noMar}}$ , as given by Eq. 4, is an estimate for a reaction time, predicted by a simple non-Markovian model, normalised by the over-damped, Markovian limit. We plot the parametrised predictions  $\xi_{\text{noMar}}$  for the set of proteins over the rescaled memory times (blue (folding) and yellow (unfolding) symbols in Fig. 4A). Except for the case of Chignolin unfolding, which is predicted to be much slower than the measured value, the agreement between the predicted folding times and those measured in the simulations is good, indicating that a simple, multi-modal, non-Markovian model describes well the accelerated barrier-crossing observed in protein folding simulations.

Reaction speed-up effects are predicted by the Grote-Hynes theory, which does not account for slow-down

effects as  $\tau_{\text{mem}} \rightarrow \infty$ , known to occur in model systems. We can contextualise the data for  $\xi$ , as given in Fig. 4A, by uniformly rescaling all time scales that enter into the heuristic formula Eq. 4 by a factor  $\alpha$ , while keeping all other parameters fixed. Such a rescaling might reflect a variation in solvent viscosity, for example. In doing so, we effectively generate an  $\alpha$ -dependent memory kernel  $\Gamma^\alpha(t) = \sum_{i=1}^M (\gamma_i/\alpha\tau_i) \exp(t/\alpha\tau_i)$ , and a corresponding effective single-valued time-scale  $\alpha\tau_{\text{mem}} = \int_0^\infty t\Gamma^\alpha(t)dt / \int_0^\infty \Gamma^\alpha(t)dt$ . In Fig. 4B, we show two examples of  $\xi(\alpha)$ , plotted as a function of  $\alpha\tau_{\text{mem}}/\tau_{\text{D}}$ . The example of Trp-Cage is particularly interesting as it shows that, in the context of this rescaling curve, the prediction for unfolding, as given in Fig. 4A and replotted as the black circle in Fig. 4B, actually coincides with the inflection from the speed-up regime, i.e.  $\xi_{\text{noMar}} < 1$ , to the kinetic slow-down regime,  $\xi_{\text{noMar}} > 1$ . This is also true of Villin and the WW-Domain (see SI - Section 8). The kinetic slow-down regime is characterised by quadratic scaling in the long memory-time limit, which is also displayed for the  $\alpha$  rescaling. Overall, the rescaling curves show that all proteins folded and unfold in the kinetic speed-up regime, which is a purely non-Markovian effect.

## DISCUSSION

We have extracted memory kernels from large-scale MD simulation trajectories of eight fast-folding proteins and found that, when measured in the  $Q$  reaction coordinate, memory times are comparable to the protein folding and unfolding reaction times, and typically vastly exceed the transition path times. It is unclear what makes a good reaction coordinate [46, 47], and such a quality is often context-dependent. For example, a reaction coordinate might be optimized such that barrier-crossing states are most likely to be transition states [48].  $Q$  has already been shown to exhibit this property [28]. But such definitions do not say anything about dynamics. In the SI (Section 9), we show examples of  $\Gamma(t)$  for other standard reaction coordinates, such as the end-to-end distance, radius of gyration, and the RMSD from the native state. The resultant memory times span orders of magnitudes but are typical of the order of the diffusion time scale  $\tau_{\text{D}}$ . Therefore, none of these reaction coordinates can be considered a good reaction coordinate, insofar as optimizing for Markovianity is a viable measure of goodness. However, we have shown that it does not matter whether we have a good or bad reaction coordinate. So long as we have the appropriate non-Markovian framework for analysing protein folding trajectories, taken from either simulation or experiments [37, 38, 40, 49, 50], we can accurately predict the folding kinetics of a protein. A simple multi-component, non-Markovian model is the most accurate for predicting the folding time’s measure in the MD simulations.

Our results indicate that, for the set of proteins considered in this paper, friction is more important than free energy barriers in determining folding times. The disclaimer is important here since the protein trajectories are drawn from a biased set, such that the proteins are selected for their short folding times, and simulation temperatures are chosen to maximize folding/unfolding transitions, i.e., the melting temperatures. Our results show that the total friction acting on  $Q$  increases more than quadratically with chain length. Barrier heights do not increase with chain length, but the barrier crossing time do (Fig. 1E-H). We cannot suggest that such dependencies hold for proteins with much larger barrier heights, or for general temperatures. Regardless, it appears that, for the present data, contributions from the friction-dependent pre-factor in the Arrhenius-type reaction-rate theories for protein folding dominate the exponential term. This is made clear when we compare Figs. 3A - C. A simple Markovian prediction for the barrier crossing times, one that only depends on friction, i.e.  $\tau_D$ , represents well the measure barrier crossing times. Explicitly accounting the exact free energy profiles makes very little improvement on this prediction. The friction is dominant. A far greater improvement is made when we account for the non-Markovian effects, as is seen in Fig. 3D.

In Eq. 3, we have only assumed constant friction. Alternative models include position-dependent friction. In the SI (Section 4), we show that for a Markovian model with position-dependent friction, there does not exist a unique friction profile  $\gamma(Q)$  for describing both folding and unfolding kinetics. This was already shown to be true for a simple  $\alpha$ -helix forming homo-alanine chain. From this we conclude that we can not predict both folding and unfolding times consistently for a given  $\gamma(Q)$ .

Whether in simulation or experiment, protein conformation dynamics must be, in general, described by some reduced-dimension collective reaction coordinate. Overall, our results suggest that, irrespective of the choice of the reaction coordinate, non-Markovian effects are present and that these effects must be taken into account when attempting to model observable features of folding proteins.

## METHODS

In Section 1 of the SI document, we present details for the molecular dynamics simulations, including various relevant simulation parameters. Additionally, we include a range of measured time-scales and other extracted quantities.

**The fraction of native contacts:** For each protein, we project the back-bone  $C_\alpha$  atomic positions from the all-atom trajectories onto the fraction of native contacts reaction coordinate  $Q$ , evaluated with a soft cut-off potential [28]. The evaluation of  $Q(t)$  requires a reference

state, which we take to be the native state for each trajectory. To evaluate the native state, we follow previous implementations and select from amongst the member states of the trajectories (as opposed to using, for example, the PDB entry). The approach is similar to that used by Lindorff-Larsen *et. al.* [22] and Best *et. al.* [28], which follows from [51]. Briefly, we sample a subset of evenly spaced states from the full trajectory. For each pair of states, we calculate the corresponding root-mean-squared deviation (RMSD) between the two states. If the RMSD between two states is less than 0.2 nm, then we place the pair into a list. We assign the state that has the most listed pairs satisfying the RMSD condition as the native state for a given protein. Note that for proteins with more than one independent trajectory segments we select a single native state from amongst all trajectory segments, which we then use for all segments. In the native state, we define all  $C_\alpha$  pairs that are separated by at least 5 residues in the primary sequence and which are separated by less than 0.9 nm in Cartesian distance, as the native contacts. Each protein will have  $N_{nc}$  native contacts.  $\mathbf{s}_{ij}^0$  are the separation vectors for all native contact pairs in the native state, which have magnitudes  $s_{ij}^0 = \sqrt{\mathbf{s}_{ij}^0 \cdot \mathbf{s}_{ij}^0}$ .  $\mathbf{s}_{ij}(t)$  are the separation vectors for all native contact pairs at each time, with magnitudes  $s_{ij}(t) = \sqrt{\mathbf{s}_{ij}(t) \cdot \mathbf{s}_{ij}(t)}$ . This gives the fraction of native contacts we deem to be in contact at time  $t$ :

$$Q(t) = \frac{1}{N_{nc}} \sum_{i < j}^{N_{nc}} \frac{1}{1 + e^{\beta(s_{ij}(t) - \gamma s_{ij}^0)}}. \quad (M1)$$

Here, we set the parameters such that  $\beta = 30 \text{ nm}^{-1}$  and  $\gamma = 1.6$ .

**Non-Markovian correction factor  $\xi_{\text{noMar}}$ :** From Kappler *et. al.* [13] and Lavacchi *et. al.* [14], we describe multi-exponential memory dependent barrier crossing times as a sum of contributions from  $M$  overdamped contributions  $\{\tau_{OD}^i\}$ , and  $M$  energy-diffusion contributions  $\{\tau_{ED}^i\}$ , where  $i = 1, 2, \dots, M$ . The individual contributions are defined as follows. For the overdamped contributions, we have:

$$\tau_{OD}^i = \tau_D \frac{\gamma_i e^{\beta U_0}}{\gamma \beta U_0} \times \left[ \frac{\pi}{2\sqrt{2}} \frac{1}{1 + 10\beta U_0 \tau_i / \tau_D} + \sqrt{\beta U_0 \frac{\tau_m}{\tau_D}} \right], \quad (M2)$$

and for the energy-diffusion contributions:

$$\tau_{ED}^i = \tau_D \frac{\gamma e^{\beta U_0}}{\gamma_i \beta U_0} \times \left[ \frac{\tau_m}{\tau_D} + 4\beta U_0 \left( \frac{\tau_i}{\tau_D} \right)^2 + \sqrt{\beta U_0 \frac{\tau_m}{\tau_D}} \right]. \quad (M3)$$



Here,  $\beta = 1/k_B T$ . We combine Eqs. M2 and M3 such that the predicted mean passage times are given by:

$$\tau_{\text{MFP}}^{\text{H}}(\tau_{\text{D}}, U_0, \{\gamma_i\}, \{\tau_i\}, \tau_{\text{m}}) = \sum_{i=1}^M \tau_{\text{OD}}^i + \left[ \sum_{i=1}^M \frac{1}{\tau_{\text{ED}}^i} \right]^{-1}. \quad (\text{M4})$$

$\{\gamma_i\}$  and  $\{\tau_i\}$  are the sets of  $M$  amplitudes and time-scales that appear in Eqs. M2 and M3. The total friction  $\gamma$  that appears in Eqs. M2 and M3 is account for since  $\gamma = \sum_{i=1}^M \gamma_i$ . The over-damped, Markovian limit is achieved by letting all memory time-scales and inertial times equal to 0. The limit is therefore given by:

$$\tau_{\text{MFP}}^{\text{H}}(\tau_{\text{D}}, U_0, \{\gamma_i\}, 0, 0) = \tau_{\text{D}} \pi U_0 e^{\beta U_0} / 2\beta \sqrt{2}, \quad (\text{M5})$$

leading to the non-Markovian correction factor  $\xi_{\text{noMar}}$  and the non-Markovian barrier crossing time  $\tau_{\text{MFP}}^{\text{noMar}}$ , as given by Eq. 4 and Eq. 5, respectively.

## ACKNOWLEDGEMENTS

We are extremely grateful to the group of David E. Shaw for providing us with the MD protein trajectories, which we have analysed in this paper. We are grateful to the physics-department HPC services at the Freie University of Berlin, for their generous provision of compute-time. This project was funded by the European Research Council (ERC) Advanced Grant 835117 NoMaMemo.

- 
- [1] J. D. Bryngelson and P. G. Wolynes, *The Journal of Physical Chemistry* **93**, 6902 (1989).
  - [2] J. D. Bryngelson, J. N. Onuchic, N. D. Socci, and P. G. Wolynes, *Proteins: Structure* **21** (1995).
  - [3] K. A. Dill and H. S. Chan, *Nature Structural Biology* **4**, 10 (1997).
  - [4] B. Schuler and W. A. Eaton, *Current Opinion in Structural Biology* **18**, 16 (2008).
  - [5] M. Hinczewski, J. C. M. Gebhardt, M. Rief, and D. Thirumalai, *Proceedings of the National Academy of Sciences* **110**, 4500 (2013).
  - [6] S. S. Plotkin and P. G. Wolynes, *Proceedings of the National Academy of Sciences* **100**, 4417 (2003).
  - [7] S. Arrhenius, *Zeitschrift für Physikalische Chemie* **4U**, 226 (1889).
  - [8] H. Eyring, *The Journal of Chemical Physics* **3**, 107 (1935).
  - [9] H. A. Kramers, *Physica* **7**, 284 (1940).
  - [10] V. I. Mel'nikov and S. V. Meshkov, *The Journal of Chemical Physics* **85**, 1018 (1986).
  - [11] R. F. Grote and J. T. Hynes, *The Journal of Chemical Physics* **73**, 2715 (1980).
  - [12] J. Kappler, J. O. Daldrop, F. N. Brünig, M. D. Boehle, and R. R. Netz, *The Journal of Chemical Physics* **148**, 14903 (2018).
  - [13] J. Kappler, V. B. Hinrichsen, and R. R. Netz, *The European Physical Journal E* **42**, 119 (2019).
  - [14] L. Lavacchi, J. Kappler, and R. R. Netz, *EPL* **131** (2020).
  - [15] I. Echeverria, D. E. Makarov, and G. A. Papoian, *Journal of the American Chemical Society* **136**, 8708 (2014).
  - [16] J. C. F. Schulz, L. Schmidt, R. B. Best, J. Dzubiella, and R. R. Netz, *Journal of the American Chemical Society* **134**, 6273 (2012).
  - [17] D. de Sancho, A. Sirur, and R. B. Best, *Nature Communications* **5**, 4307 (2014).
  - [18] O. F. Lange and H. Grubmüller, *The Journal of Chemical Physics* **124**, 214903 (2006).
  - [19] R. B. Best and G. Hummer, *Physical Review Letters* **96**, 228104 (2006).
  - [20] R. B. Best and G. Hummer, *Proceedings of the National Academy of Sciences* **107**, 1088 LP (2010).
  - [21] M. Hinczewski, Y. von Hansen, J. Dzubiella, and R. R. Netz, *The Journal of Chemical Physics* **132**, 245103 (2010).
  - [22] K. Lindorff-Larsen, S. Piana, R. O. Dror, and D. E. Shaw, *Science* **334**, 517 LP (2011).
  - [23] D. E. Shaw, R. O. Dror, J. K. Salmon, J. P. Grossman, K. M. Mackenzie, J. A. Bank, C. Young, M. M. Denieroff, B. Batson, K. J. Bowers, E. Chow, M. P. Eastwood, D. J. Ierardi, J. L. Klepeis, J. S. Kuskin, R. H. Larson, K. Lindorff-Larsen, P. Maragakis, M. A. Moraes, S. Piana, Y. Shan, and B. Towles, in *Proceedings of the Conference on High Performance Computing Networking, Storage and Analysis* (2009) pp. 1–11.
  - [24] D. E. Shaw, P. Maragakis, K. Lindorff-Larsen, S. Piana, R. O. Dror, M. P. Eastwood, J. A. Bank, J. M. Jumper, J. K. Salmon, Y. Shan, and W. Wriggers, *Science (New York, N.Y.)* **330**, 341 (2010).
  - [25] R. Zwanzig, *Physical Review* **124**, 983 (1961).
  - [26] H. Mori, *Progress of Theoretical Physics* **33**, 423 (1965).
  - [27] H. Nymeyer, A. E. García, and J. N. Onuchic, *Proceedings of the National Academy of Sciences* **95**, 5921 (1998).
  - [28] R. B. Best, G. Hummer, and W. A. Eaton, *Proceedings of the National Academy of Sciences* **110**, 17874 LP (2013).
  - [29] C. Ayaz, L. Scalfi, B. A. Dalton, and R. R. Netz, *Physical Review E* **105**, 54138 (2022).
  - [30] J. E. Straub, M. Borkovec, and B. J. Berne, *The Journal of Physical Chemistry* **91**, 4995 (1987).
  - [31] J. O. Daldrop, J. Kappler, F. N. Brünig, and R. R. Netz, *Proceedings of the National Academy of Sciences* **115**, 5169 (2018).
  - [32] E. Darve, J. Solomon, and A. Kia, *Proceedings of the National Academy of Sciences* **106**, 10884 (2009).
  - [33] C. Ayaz, L. Tepper, F. N. Brünig, J. Kappler, J. O. Daldrop, and R. R. Netz, *Proceedings of the National Academy of Sciences* **118**, e2023856118 (2021).
  - [34] B. Kowalik, J. O. Daldrop, J. Kappler, J. C. F. Schulz, A. Schlaich, and R. R. Netz, *Physical Review E* **100**, 12126 (2019).
  - [35] T. R. Einert, C. E. Sing, A. Alexander-Katz, and R. R. Netz, *The European Physical Journal. E, Soft Matter* **34**, 1 (2011).

- [36] P. G. de Gennes, *The Journal of Chemical Physics* **55**, 572 (1971).
- [37] H. S. Chung and W. A. Eaton, *Nature* **502**, 685 (2013).
- [38] C. H. Sung, M. Kevin, L. J. M., and E. W. A., *Science* **335**, 981 (2012).
- [39] H. S. Chung, S. Piana-Agostinetti, D. E. Shaw, and W. A. Eaton, *Science (New York, N.Y.)* **349**, 1504 (2015).
- [40] N. Krishna, F. D. A. N., D. D. R., Y. Hao, W. Feng, and W. M. T., *Science* **352**, 239 (2016).
- [41] R. Satija, A. Das, and D. E. Makarov, *The Journal of Chemical Physics* **147**, 152707 (2017).
- [42] J. O. Daldrop, W. K. Kim, and R. R. Netz, *EPL (Europhysics Letters)* **113**, 18004 (2016).
- [43] G. Hummer, *The Journal of Chemical Physics* **120**, 516 (2003).
- [44] M. Laleman, E. Carlon, and H. Orland, *The Journal of Chemical Physics* **147**, 214103 (2017).
- [45] E. Carlon, H. Orland, T. Sakaue, and C. Vanderzande, *The Journal of Physical Chemistry B* **122**, 11186 (2018).
- [46] A. Sali, E. Shakhnovich, and M. Karplus, *Nature* **369**, 248 (1994).
- [47] R. Du, V. S. Pande, A. Y. Grosberg, T. Tanaka, and E. S. Shakhnovich, *The Journal of Chemical Physics* **108**, 334 (1998).
- [48] R. B. Best and G. Hummer, *Proceedings of the National Academy of Sciences* **102**, 6732 LP (2005).
- [49] M. Pirchi, R. Tsukanov, R. Khamis, T. E. Tomov, Y. Berger, D. C. Khara, H. Volkov, G. Haran, and E. Nir, *The Journal of Physical Chemistry B* **120**, 13065 (2016).
- [50] H. Y. Aviram, M. Pirchi, H. Mazal, Y. Barak, I. Riven, and G. Haran, *Proceedings of the National Academy of Sciences* **115**, 3243 (2018).
- [51] X. Daura, K. Gademann, B. Jaun, D. Seebach, W. F. van Gunsteren, and A. E. Mark, *Angewandte Chemie International Edition* **38**, 236 (1999).